Cell stimulation with optically manipulated microsources

Holger Kress[1], Jin-Gyu Park[1], Cecile O Mejean[1], Jason D Forster[1], Jason Park[2], Spencer S Walse[3,8], Yong Zhang[4], Dianqing Wu[4], Orion D Weiner[5], Tarek M Fahmy[2,3] & Eric R Dufresne[1,3,6,7]

Molecular gradients are important for various biological processes including the polarization of tissues and cells during embryogenesis and chemotaxis. Investigations of these phenomena require control over the chemical microenvironment of cells. We present a technique to set up molecular concentration patterns that are chemically, spatially and temporally flexible. Our strategy uses optically manipulated microsources, which steadily release molecules. Our technique enables the control of molecular concentrations over length scales down to about 1 μm and timescales from fractions of a second to an hour. We demonstrate this technique by manipulating the motility of single human neutrophils. We induced directed cell polarization and migration with microsources loaded with the chemoattractant formyl-methionine-leucine-phenylalanine. Furthermore, we triggered highly localized retraction of lamellipodia and redirection of polarization and migration with microsources releasing cytochalasin D, an inhibitor of actin polymerization.

Gradients of molecules are important for cell differentiation during embryonic development[1,2], for food gathering of single cellular organisms[3–5] and for the immune response of higher organisms[6]. Chemotaxis, the directed migration of a cell along a chemical gradient, is a key element of the mammalian immune system[4,5,7,8]. Prokaryotes and eukaryotes have different mechanisms of chemotaxis: whereas bacteria temporally sense gradients and exhibit a biased random walk[3], eukaryotes can spatially sense gradients and regulate the actin cytoskeleton to migrate toward sources of chemoattractant[4,5,7,8]. Over the past decade, mathematical models of eukaryotic chemotaxis have matured and incorporated various biochemical reaction-diffusion schemes[9,10]. Different models describe qualitatively different modes of gradient sensing and show qualitatively different spatial and temporal dynamics. To test predictions from competing models in experiments, precise control over chemical microenvironments of cells is needed.

Established techniques to create linear or radial gradients of soluble molecules have used diffusion chambers and micropipettes. Emerging techniques that incorporate microfluidic devices[11,12], photoinduced uncaging[12,13] or photolysis of nanoparticles[14] allow more control over the geometry and the dynamics of the molecular concentration patterns. However, there is so far no technique available that allows the creation of persistent gradient patterns that can be flexibly shaped in three dimensions down to micrometer scales.

Here we present a strategy for cell stimulation that enables the control of concentrations of soluble molecules over length scales from about 100 μm to 1 μm at timescales from hours to a fraction of a second. This strategy is based on optically manipulated microsources (OMMs), microparticles that provide a controlled release of soluble molecules that act as chemoattractants or perturb the actin cytoskeleton. We individually trapped multiple microsources and independently manipulated them with holographic optical tweezers[15–17].

RESULTS

Microsource fabrication and structure

We fabricated microsources releasing the chemoattractant formyl-methionine-leucine-phenylalanine (fMLP; 438 g mol^{-1}) and microsources releasing the actin polymerization inhibitor cytochalasin D (508 g mol^{-1})[18,19] from polylactic-co-glycolic acid (PLGA) using a solvent evaporation–spontaneous emulsion technique[20]. Particles releasing fMLP stimulated chemotactic responses in single neutrophil-differentiated HL-60 cells, and particles releasing cytochalasin D perturbed the actin cytoskeleton of single HL-60 cells with high spatial localization.

The nominal loading (mass of the loaded chemical divided by the total mass of the loaded chemical and PLGA) was 0.01–0.17. We measured the structure of the PLGA particles by scanning electron microscopy (SEM). The SEM image (**Supplementary Fig. 1**) revealed that the particles were spherical. We measured the size distribution of the beads by SEM and by dynamic light scattering. The particles had a mean diameter of 500–1,000 nm and an average polydispersity (s.d. of diameter divided by mean diameter) of ~40%.

[1]Department of Mechanical Engineering, [2]Department of Biomedical Engineering and [3]Department of Chemical Engineering, Yale University, New Haven, Connecticut, USA. [4]Vascular Biology and Therapeutics Program and Department of Pharmacology, Yale University School of Medicine, New Haven, Connecticut, USA. [5]Department of Biochemistry, University of California, San Francisco, San Francisco, California, USA. [6]Department of Physics and [7]Department of Cell Biology, Yale University New Haven, Connecticut, USA. [8]Present address: US Department of Agriculture, Parlier, California, USA. Correspondence should be addressed to H.K. (holger.kress@yale.edu) or E.R.D. (eric.dufresne@yale.edu).

RECEIVED 2 SEPTEMBER; ACCEPTED 13 OCTOBER; PUBLISHED ONLINE 15 NOVEMBER 2009; DOI:10.1038/NMETH.1400

Controlled release of encapsulated agents

We determined the concentration profile of molecules released from a microsource close to a coverslip by the release rate, the diffusion coefficient of the released molecule and the boundary condition imposed by the impenetrable coverslip. The concentration profile around a particle at a height h above a coverslip was approximated (derivation in **Supplementary Note 1**) by

$$c(\rho,z) = c_b + c_0 \times a\left(\frac{1}{\left(\rho^2+(z+h)^2\right)^{\frac{1}{2}}}+\frac{1}{\left(\rho^2+(z-h)^2\right)^{\frac{1}{2}}}\right) \quad (1)$$

in which a is the particle radius, ρ and z are the cylindrical coordinates, c_0 is the concentration on the surface of the bead and c_b is the homogeneous background concentration. The concentration on the surface of the bead,

$$c_0 = j_0 \times \frac{a}{D} \quad (2)$$

was determined by the flux, j_0, of molecules from the particle surface and the diffusion coefficient, D, of the molecules. This equation is only exact when $h \gg a$. An example for a concentration profile around a particle is shown in **Supplementary Figure 2**.

To estimate the flux from individual beads, we measured the release of fMLP from ensembles of PLGA beads (**Supplementary Note 1**). Beads at a concentration of 1 mg ml^{-1} released 60 µM of fMLP during the first hour after suspending the beads in buffer solution. Release measurements on individual PLGA particles loaded with the fluorescent dye rhodamine B showed that the release rate was proportional to the bead volume (**Supplementary Note 2** and **Supplementary Fig. 3**). Assuming the same particle size–dependence for fMLP yielded a flux of j_0 = 5,000 molecules µm^{-2} s^{-1} (60,000 molecules per second) from a microsource with a diameter of 2 µm. Using equation 2 and the diffusion coefficient of fMLP, D = ~1,000 µm^2 s^{-1}, the estimated concentration on the surface of the bead was therefore c_0 = 8 nM.

The concentration distribution of fMLP around a single microsource was sufficient to induce chemotaxis. If a 2-µm bead were placed near the membrane of a cell with a diameter of 20 µm, the cell would be exposed to an fMLP concentration of about 8 nM at the side facing the bead and a concentration of 0.2 nM at the opposite side if no homogeneous background concentration was present. If the background concentration is the dissociation constant (K_d) (~10 nM) for fMLP binding to its receptor[11], the front of the cell is exposed to an 80% larger concentration than the back of the cell. Concentration differences on that order of magnitude at an ambient concentration with a value of approximately the K_d value can induce chemotaxis in neutrophils[11].

Cell response to microsources of chemoattractants

Differentiated HL-60 cells are a neutrophil-like cell line that is used as a model system for studying neutrophil chemotaxis[21]. In positive control experiments, we characterized the migration of HL-60 cells in gradients of fMLP in a Zigmond diffusion chamber[22]. The potency of fMLP to stimulate chemotaxis was not reduced when it was encapsulated and released from PLGA beads (**Supplementary Note 3** and **Supplementary Fig. 4**). By using HL-60 cells transfected with *YFP-actin* plasmid, we found that freely diffusing fMLP-loaded PLGA beads induced cell polarization and actin accumulation (**Supplementary Fig. 5**).

Individual optically trapped PLGA microparticles loaded with fMLP could induce a chemotactic response in single neutrophils. We introduced the microparticles to samples of HL-60 cells plated on coverslips and imaged the cells by differential interference contrast microscopy. We assayed the interaction of a cell with a single fMLP-loaded particle manipulated with holographic optical tweezers (**Fig. 1** and **Supplementary Video 1**). We moved an individual fMLP-loaded particle close to the membrane of a neutrophil (**Fig. 1a**). The cell started to polarize

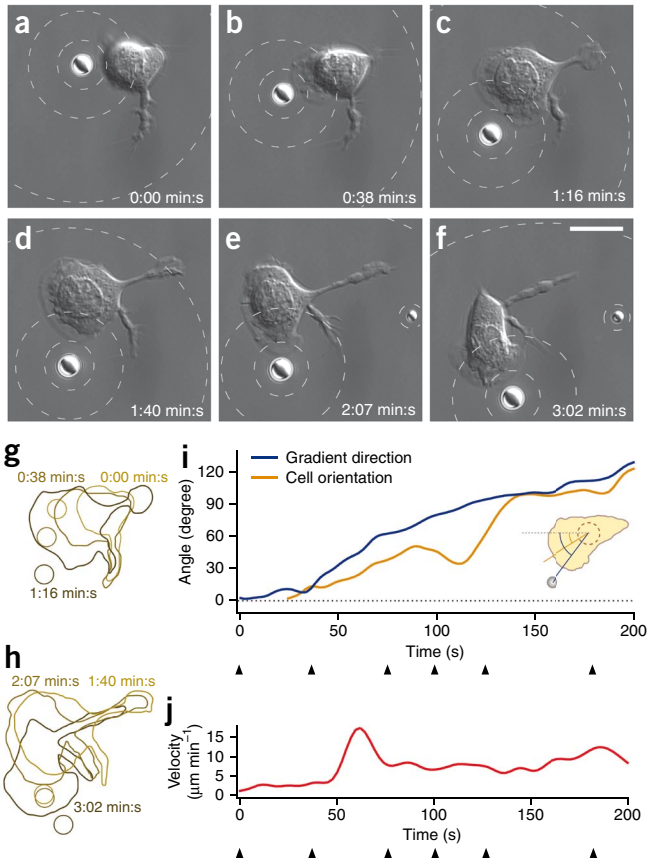

Figure 1 | A single optically manipulated bead loaded with chemoattractant induces directed polarization and migration of a neutrophil. (**a**–**f**) Differential interference contrast (DIC) microscopy images. PLGA particle loaded with fMLP was moved close to the membrane of an HL-60 cell (**a**). Cell polarized and migrated in the direction of the particle (**b**). Particle was moved counter-clockwise around the cell and the cell changed polarization and migration direction (**c**–**f**). The dashed contour lines indicate the spatially varying concentration of fMLP around the bead. The concentration on the surface of the bead (c_0) was 2 nM above the background, c_b = 20 nM. The contour lines show fMLP concentration levels of 50%, 25% and 10% of c_0 above c_b. Scale bars, 10 µm. (**g**,**h**) Sketches showing the cell contour and the bead contour from the images in **a**–**f** (split into two sketches for clarity). The different colors of the contours indicate the different time points of the image series. (**i**,**j**) Direction of the gradient and cell orientation (direction from the center of the cell to the center of the leading edge) (**i**) and cell velocity (**j**) as a function of time. The directions were quantified as angles with respect to the dashed reference line. Arrowheads mark the time points shown in **a**–**f**.

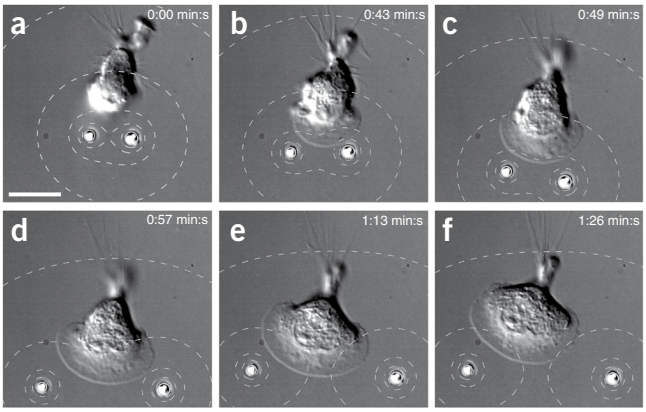

Figure 2 | Bipolar stimulation with chemoattractant induced formation and broadening of a lamellipodium. (**a**–**d**) Upon positioning of fMLP-loaded beads close to a HL-60 cell (**a**), the cell formed a lamellipodium in the direction of the beads (**b**) that broadened as the cell advanced toward the beads (**c**,**d**). (**e**,**f**) Ultimately, the lamellipodium reached its maximal size and the cell oriented toward the lower left bead. The contour lines in the DIC images show fMLP concentration (80, 60, 40, 20 and 10% of c_0 = 1 nM above the background c_b = 10 nM). Scale bars, 10 μm.

and migrate in the direction of the particle (**Fig. 1b**). We then moved the particle counter-clockwise around the cell, and the cell changed its polarization and migration directions in response to the altered particle position (**Fig. 1c–f**). We estimated fMLP concentration around the bead (**Fig. 1**). The influence of the motion of the bead on the concentration pattern was negligible. In this and subsequent cell stimulation experiments, we moved the particles at speeds not exceeding 1 μm s^{-1}. At such low speeds, the steady-state solution (equation 1) was a good approximation for the concentration distribution at any time (**Supplementary Note 4**). Furthermore, the presence of a cell changed the concentration pattern around a bead only negligibly (**Supplementary Note 5** and **Supplementary Fig. 6**).

We analyzed the time-dependent orientation and motion of the cell (**Fig. 1g,h**) to determine whether it followed the bead motion: we extracted the cell position, the direction of the cell orientation and the direction of the gradient of fMLP from each of the time-lapse images. The angle that quantified the direction of the gradient increased continuously with time (**Fig. 1i**). The cell orientation could not be defined at the earliest time points (time $t \leq 25$ s) because the cell was lacking a leading edge. After the cell created a leading edge, the cell orientation followed the gradient direction with a time delay of up to 60 s. The cell responded to the stimulus created by the bead by polarizing and migrating in the direction of the stimulus. Upon first exposure to the bead, the cell reached a peak velocity of more than 15 μm min^{-1}, which decreased to ~7–13 μm min^{-1} for the remainder of the experiment (**Fig. 1j**). An additional movie of a single HL-60 cell stimulation with an individual optically trapped PLGA particle loaded with fMLP is shown in **Supplementary Video 2**.

The capability to trap and manipulate multiple microsources simultaneously offers a high degree of spatial flexibility for the creation of cell stimulus patterns that are not easily achieved with micropipettes. We assayed the response of a single HL-60 cell to a highly localized bipolar stimulus created with two optically trapped beads releasing fMLP (**Fig. 2** and **Supplementary Video 3**). Upon positioning of the beads close to the cell, the cell formed a lamellipodium, which broadened as it advanced toward the well-separated beads.

Control experiments with optically manipulated unloaded PLGA beads showed no chemotactic response of the cells (**Supplementary Videos 4** and **5**). Furthermore, we quantified the heating of the trapped particles owing to the laser tweezers by using the temperature-dependent fluorescent dye Rhodamine B. The intensity of the fluorescence emitted from Rhodamine B decreases by 2.3% per 1 °C temperature increase[23]. For the trapping powers used in this study (~5 mW) the particles heated up by less than 0.1 °C (**Supplementary Note 6** and **Supplementary Fig. 7**). As the plain PLGA beads did not affect the cell behavior, this temperature increase is negligible.

Cell response to actin polymerization inhibitors

We manipulated the motility of neutrophils using beads releasing the actin polymerization inhibitor cytochalasin D in the presence of a homogeneous background concentration of 100 nM fMLP. OMMs created highly localized stimuli, which induced strongly localized cytoskeletal perturbations (**Fig. 3** and **Supplementary Video 6**). We stimulated an HL-60 cell with two optically trapped beads releasing cytochalasin D. We positioned the beads close to each other and to the center of the lamellipodium. After about 45 s, the lamellipodium started to retract at 10 μm min^{-1} in a small region around the beads. As a result, the lamellipodium was initially split into two parts. About 1 minute after the split, one of the two lamellipodia retracted while the other one persisted.

Bipolar perturbations caused notable changes to cell motility. We positioned two beads, separated by ~20 μm, in front of a migrating

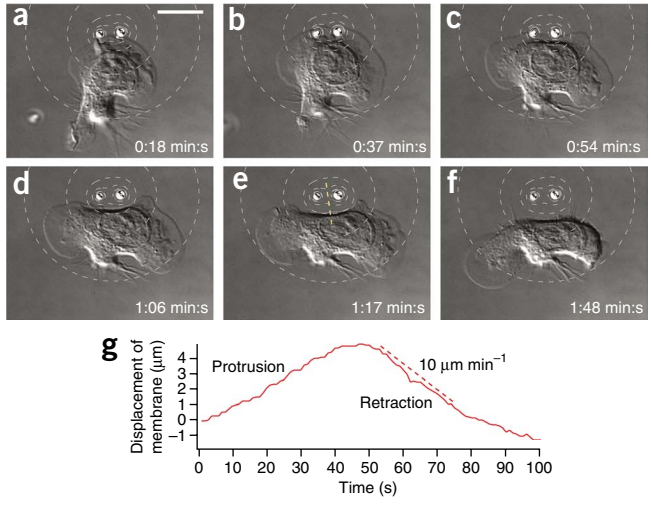

Figure 3 | OMMs of cytochalasin D induced highly localized retraction in the center of a lamellipodium. (**a**,**b**) Two beads releasing cytochalasin D close to the center of the lamellipodium of a migrating HL-60 cell. (**c**–**e**) Lamellipodium retracted in a small region around the beads (**c**) yielding a lamellipodium that was split into two parts (**d**,**e**). (**f**) Only one lamellipodium remained. The contour lines in the DIC images show cytochalasin D concentration (80, 60, 40, 20 and 10% of c_0 above the background). Scale bars, 10 μm. (**g**) The displacement of the membrane along the dashed yellow line in **e**.

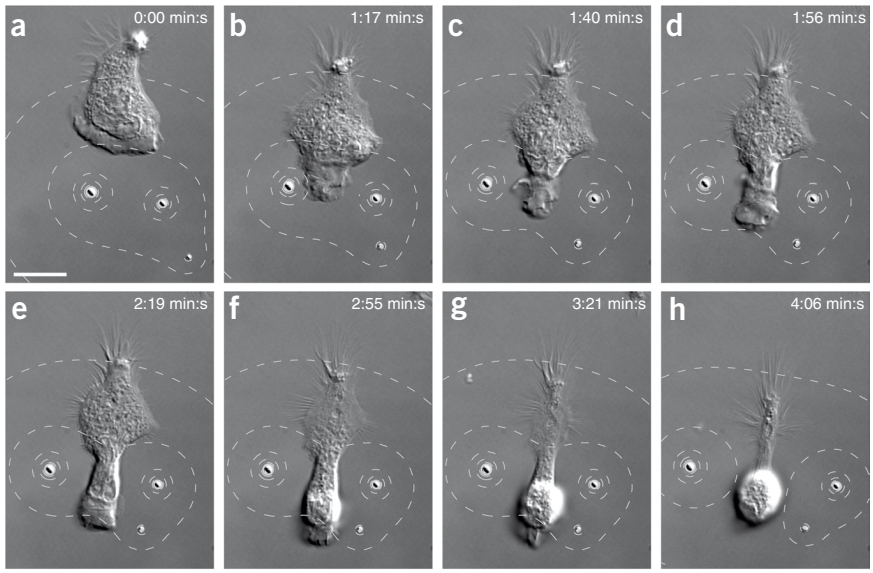

Figure 4 | Migrating cell squeezes between two optically manipulated microsources of cytochalasin D. (**a**) Two beads in front of a migrating HL-60 cell. (**b**–**f**) As the bead-to-bead distance increased to about 20 μm, the lamellipodium of the cell migrating toward the two particles retracted on the two sides closest to the beads while the central part of the leading edge continues to extend. (**g**,**h**) The cell rounded up and retracted its leading edge. The contour lines in the DIC images show cytochalasin D concentration (80, 60, 40, 20 and 10% of c_0 above background). Scale bars, 10 μm.

cell (**Fig. 4** and **Supplementary Video 7**). The cell squeezed through the narrow gap created by the two microsources: the lamellipodium retracted on the two sides closest to the beads while the central part of the lamellipodium continued to progress. To analyze the response of an HL-60 cell to a temporally varying bipolar perturbation with cytochalasin D, we first stopped cell migration with two microsources (**Fig. 5a**,**b** and **Supplementary Video 8**). Then, we repositioned the two beads on two opposing ends of the cell along the direction of cell polarization. Subsequently, the cell repolarized in a direction perpendicular to the axis defined by the beads (**Fig. 5c**–**f**).

Holographic optical tweezers provide a high degree of spatial flexibility for the creation of molecular concentration patterns through their ability to independently manipulate multiple particles. We assayed this flexibility by stimulating single cells simultaneous with three or five microsources (**Supplementary Fig. 8**). Furthermore, the dynamic reconfiguration of optical traps provided a high degree of temporal flexibility. Our holographic optical tweezers[17] setup allowed us to move individual microsources independently of each other at speeds up to 25 μm s^{-1}. Therefore it was possible to switch within about 1 s between well-defined spatial stimulation patterns on length scales of tens of micrometers. One second was enough time for the concentration distribution around a bead to reach steady state (**Supplementary Note 4**).

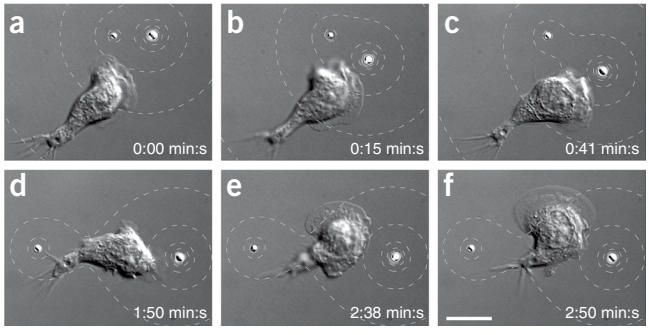

Figure 5 | Response of HL-60 cells to time-varying bipolar stimulus of cytochalasin D. (**a**–**c**) The cell stopped its migration and retracted its lamellipodium in response to two microsources of cytochalasin D placed in the direction of cell migration. (**d**) The two beads positioned on two opposing ends of the cell in the direction of cell polarization. (**e**,**f**) The cell repolarized in a direction perpendicular to the axis defined by the beads. The contour lines in the DIC images show cytochalasin D concentration (80, 60, 40, 20 and 10% of c_0 above background). Scale bars, 10 μm.

DISCUSSION

The length scale of the chemical concentration patterns that can be generated by our technique depends on various factors. On the lower end, it is determined by the size of the particles that are releasing the stimulus. On the upper end, it is determined by the size of the microscope field of view in which particles can be optically manipulated and also by the number of particles that can be trapped simultaneously. Here we used particles with radii of 1.5–4 μm. Holographic optical tweezers setups allow trapping of about 100 particles simultaneously. Packing particles close together (particles with a diameter larger than about 1 μm can be packed to contact) allows mimicking large sources of chemoattractant with multiple small beads. The possibility to vary the size of microsources allows investigation of the response of cells to stimuli that vary in their degree of localization. For example, it has been found that localized release of cytokines from microparticles can induce a response in T cells that is different from the response to exogenous addition of cytokines[24]. Therefore, OMMs could, for example, enable further investigation into how paracrine delivery of agents may impact immune system cell function.

In addition to using multiple beads to create flexible spatial stimulation, we applied flexible temporal stimulation patterns to a cell by dynamically changing the distance of one or more beads away from the cell. The maximal frequency of stimulation we can create by our current implementation of holographic optical tweezers is about 30 Hz, which can be transmitted over a range of about 10 μm. However, if necessary, much larger stimulation frequencies could be generated with devices such as acousto-optical deflectors that can be driven in the range of kHz and above. Over larger distances, the maximal frequency that can be transmitted decreases (**Supplementary Note 4**).

Finally, OMMs offer a high degree of chemical flexibility. The PLGA particles that we used here trap the encapsulated molecules physically during the particle fabrication process. This enables the encapsulation and controlled release of a large variety

of molecules including proteins, small peptides, fluorescent dyes, oligonucleotides and small-molecule drugs[20,25]. In contrast, caged molecules require the chemical development of a caged version for each type of molecule. Furthermore, PLGA is a well-established material that has no adverse side effects on cellular viability[26,27]. However, PLGA microparticles had been designed for release over long periods of time with large numbers of particles. Further optimization, including the use of other materials such as colloidosomes[28] and mesoporous silica nanoparticles[29,30], could potentially increase the concentration of released molecules by two orders of magnitude (**Supplementary Note 7**).

The spatial, temporal and chemical flexibility of OMMs make them applicable to a broad range of research areas in cell and developmental biology, where it is of interest to stimulate single cells or developing organisms locally with specific molecules.

METHODS

Methods and any associated references are available in the online version of the paper at http://www.nature.com/naturemethods/.

Note: Supplementary information is available on the Nature Methods website.

ACKNOWLEDGMENTS

We thank S. Dandekar, A. Houk, A. Millius and S. Wilson for help with cell culturing and sample preparation, A. Schaefer for helpful discussions, and M. Elimelech and W. Mitch for use of equipment. This work was supported by a fellowship (BMBF-LPD 9901/8-162) from the German Academy of Sciences Leopoldina to H.K., a US National Institutes of Health grant (1U54-RR0222332) and US National Science Foundation grants (CBET-0619674 and DBI–0619674) to E.R.D., a US National Institutes of Health grant (RO1-GM084040) to O.D.W and a US National Science Foundation CAREER grant (CBET-0747577) to T.M.F.

AUTHOR CONTRIBUTIONS

H.K. and E.R.D. designed and performed the research, analyzed data and wrote the paper. J.G.P., J.D.F., S.S.W. and O.D.W. performed research and analyzed data. C.O.M. and Y.Z. performed research. J.P. and T.M.F. designed research and contributed new reagents and analytic tools. D.W. designed research.

Published online at http://www.nature.com/naturemethods/.
Reprints and permissions information is available online at http://npg.nature.com/reprintsandpermissions/.

1. Gurdon, J.B. & Bourillot, P.Y. Morphogen gradient interpretation. *Nature* **413**, 797–803 (2001).
2. Meinhardt, H. Models of biological pattern formation: from elementary steps to the organization of embryonic axes. *Curr. Top. Dev. Biol.* **81**, 1–63 (2008).
3. Wadhams, G.H. & Armitage, J.P. Making sense of it all: bacterial chemotaxis. *Nat. Rev. Mol. Cell Biol.* **5**, 1024–1037 (2004).
4. Kay, R.R., Langridge, P., Traynor, D. & Hoeller, O. Changing directions in the study of chemotaxis. *Nat. Rev. Mol. Cell Biol.* **9**, 455–463 (2008).
5. Van Haastert, P.J.M. & Devreotes, P.N. Chemotaxis: signalling the way forward. *Nat. Rev. Mol. Cell Biol.* **5**, 626–634 (2004).
6. Cyster, J.G. Chemokines and cell migration in secondary lymphoid organs. *Science* **286**, 2098–2102 (1999).
7. Weiner, O.D. Regulation of cell polarity during eukaryotic chemotaxis: the chemotactic compass. *Curr. Opin. Cell Biol.* **14**, 196–202 (2002).
8. Parent, C.A. & Devreotes, P.N. A cell's sense of direction. *Science* **284**, 765–770 (1999).
9. Iglesias, P.A. & Levchenko, A. Modeling the cell's guidance system. *Sci. STKE* **2002**, re12 (2002).
10. Skupsky, R., Losert, W. & Nossal, R.J. Distinguishing modes of eukaryotic gradient sensing. *Biophys. J.* **89**, 2806–2823 (2005).
11. Herzmark, P. *et al.* Bound attractant at the leading vs. the trailing edge determines chemotactic prowess. *Proc. Natl. Acad. Sci. USA* **104**, 13349–13354 (2007).
12. Beta, C., Wyatt, D., Rappel, W.J. & Bodenschatz, E. Flow photolysis for spatiotemporal stimulation of single cells. *Anal. Chem.* **79**, 3940–3944 (2007).
13. Samadani, A., Mettetal, J. & van Oudenaarden, A. Cellular asymmetry and individuality in directional sensing. *Proc. Natl. Acad. Sci. USA* **103**, 11549–11554 (2006).
14. Sun, B.Y. & Chiu, D.T. Synthesis, loading, and application of individual nanocapsules for probing single-cell signaling. *Langmuir* **20**, 4614–4620 (2004).
15. Dufresne, E.R. & Grier, D.G. Optical tweezer arrays and optical substrates created with diffractive optics. *Rev. Sci. Instrum.* **69**, 1974–1977 (1998).
16. Dufresne, E.R., Spalding, G.C., Dearing, M.T., Sheets, S.A. & Grier, D.G. Computer-generated holographic optical tweezer arrays. *Rev. Sci. Instrum.* **72**, 1810–1816 (2001).
17. Mejean, C.O., Schaefer, A.W., Millman, E.A., Forscher, P. & Dufresne, E.R. Multiplexed force measurements on live cells with holographic optical tweezers. *Opt. Express* **17**, 6209–6217 (2009).
18. Cooper, J.A. Effects of cytochalasin and phalloidin on actin. *J. Cell Biol.* **105**, 1473–1478 (1987).
19. Urbanik, E. & Ware, B.R. Actin filament capping and cleaving activity of cytochalasin-B, cytochalasin-D, cytochalasin-E and cytochalasin-H. *Arch. Biochem. Biophys.* **269**, 181–187 (1989).
20. Fahmy, T.M., Samstein, R.M., Harness, C.C. & Saltzman, W.M. Surface modification of biodegradable polyesters with fatty acid conjugates for improved drug targeting. *Biomaterials* **26**, 5727–5736 (2005).
21. Servant, G. *et al.* Polarization of chemoattractant receptor signaling during neutrophil chemotaxis. *Science* **287**, 1037–1040 (2000).
22. Zigmond, S.H. Ability of polymorphonuclear leukocytes to orient in gradients of chemotactic factors. *J. Cell Biol.* **75**, 606–616 (1977).
23. Ebert, S., Travis, K., Lincoln, B. & Guck, J. Fluorescence ratio thermometry in a microfluidic dual-beam laser trap. *Opt. Express* **15**, 15493–15499 (2007).
24. Steenblock, E.R. & Fahmy, T.M. A comprehensive platform for *ex vivo* T-cell expansion based on biodegradable polymeric artificial antigen-presenting cells. *Mol. Ther.* **16**, 765–772 (2008).
25. Vasir, J.K. & Labhasetwar, V. Biodegradable nanoparticles for cytosolic delivery of therapeutics. *Adv. Drug Deliv. Rev.* **59**, 718–728 (2007).
26. Cohen, S., Yoshioka, T., Lucarelli, M., Hwang, L.H. & Langer, R. Controlled delivery systems for proteins based on poly(lactic/glycolic acid) microspheres. *Pharm. Res.* **8**, 713–720 (1991).
27. Jiang, W.L., Gupta, R.K., Deshpande, M.C. & Schwendeman, S.P. Biodegradable poly(lactic-co-glycolic acid) microparticles for injectable delivery of vaccine antigens. *Adv. Drug Deliv. Rev.* **57**, 391–410 (2005).
28. Dinsmore, A.D. *et al.* Colloidosomes: selectively permeable capsules composed of colloidal particles. *Science* **298**, 1006–1009 (2002).
29. Slowing, I.I., Trewyn, B.G., Giri, S. & Lin, V.S.Y. Mesoporous silica nanoparticles for drug delivery and biosensing applications. *Adv. Funct. Mater.* **17**, 1225–1236 (2007).
30. Carroll, N.J. *et al.* Droplet-based microfluidics for emulsion and solvent evaporation synthesis of monodisperse mesoporous silica microspheres. *Langmuir* **24**, 658–661 (2008).

ONLINE METHODS

Cell culture. HL-60 cells were grown in RPMI 1640 (with L-glutamine, Cellgro) with 25 mM Hepes (Hepes solution, cell culture–tested; Sigma), 10% FBS (certified and heat-inactivated; Invitrogen) and 1% antibiotic-antimycotic (100×, Invitrogen). The cells were differentiated with growth medium containing 1.3% DMSO (Hybri-Max, sterile-filtered and hybridoma tested; Sigma) 5–8 d before the microscopy experiments.

PLGA microparticle fabrication. Polylactic-co-glycolic acid (PLGA) 50/50 had a molecular weight of approximately 10^5 g mol^{-1}, which corresponds to an inherent viscosity of 0.95–1.10 dl g^{-1} in hexafluoroisopropanol (Absorbable Polymers; Durect Corporation). N-formyl-Met-Leu-Phe (fMLP), CD, polyvinylalcohol (PVA, 87–89% hydrolyzed, 30,000–70,000 g mol^{-1}), dimethyl sulfoxide (DMSO), methylene chloride (DCM) had reagent-grade or higher and were used without further purification (all purchased from Sigma-Aldrich).

PLGA microparticles loaded with fMLP or CD were prepared using a solvent evaporation–spontaneous emulsion technique[20]. For particles with 9% nominal loading of fMLP, 10 mg of lyophilized fMLP powder was added directly to a PLGA solution of 100 mg polymer in 2 ml of DCM. For particles with 17% nominal loading of fMLP, 20 mg of lyophilized fMLP powder was added directly to a PLGA solution of 100 mg polymer in 2 ml of DCM. For particles with 1% nominal loading of fMLP, fMLP was dissolved at a concentration of 5 mg ml^{-1} in PBS and 200 µl of this solution was added to a PLGA solution of 100 mg polymer in 2 ml of DCM. For particles with 9% nominal loading of CD, 5 mg of CD were dissolved in 1 ml of DCM and added to a PLGA solution of 50 mg polymer in 1 ml of DCM.

When the fMLP powder was added directly to the PLGA solution, the solution was sonicated on ice twice for 10 s at 38% amplitude (GEX600 600 W ultrasonic processor). This step was omitted when the fMLP or the cytochalasin was dissolved before adding it to the PLGA solution. The PLGA solution was added dropwise under vortexing to 4 ml (2 ml in case of the cytochalasin beads) of 1 wt% PVA aqueous solution. The mixture was sonicated for 2 × 10 s on ice at 38% amplitude. The resulting oil-in-water droplets were hardened by evaporating the DCM in 200 ml (75 ml in the case of the cytochalasin beads) of 0.3 wt% of PVA aqueous solution with magnetic stirring for 3 h at room temperature (20–22 °C). The particles were washed three times by centrifugation at 12,000*g* for 5 min and then recovered by lyophilization and stored at −20 °C.

Scanning electron microscopy. The morphology of the fMLP-loaded PLGA particles was measured by scanning electron microscopy (SEM). Particles were fixed on an aluminum stub using two-sided carbon tape and sputter-coated with gold under vacuum in an argon atmosphere at a sputter current of 40 mA (model 108auto; Cressington). The samples were then imaged using a Philips XL-30 ESEM with 10 kV of accelerating voltage.

Dynamic light scattering. Particle sizes were measured by dynamic light scattering using a Brookhaven ZetaPALS system equipped with a particle sizer (Brookhaven Instruments Corporation). The particles were diluted to 0.01 mg ml^{-1} in DI water to give an average count rate of 200,000 c.p.s. before testing. Correlation functions were collected at a scattering angle of 90° (incident beam wavelength, 532 nm). Then the effective diameter and polydispersity of the particle were calculated using the manufacturer's particle sizing software (version 2.27).

Release measurements. PLGA beads loaded with fMLP samples were prepared by dispersing in HBSS at a concentration of 5 mg ml^{-1}. We added 200 µl of this solution into a 1.5 ml microcentrifuge tube for each time point (5, 30, 60 min and so forth) of the release curve (**Supplementary Fig. 2b**). At the respective time points, the tube was centrifuged at 2,300*g* for 3 min and 150 µl of the supernatant was collected. The supernatant was then either used undiluted for an ultraviolet (UV) fluorescence spectroscopy measurement of the fMLP concentration or diluted 1:100 for a high-performance liquid chromatography measurement of the fMLP concentration.

High-performance liquid chromatography was done using a Thermo Separation Products Spectra system P4000 pump, ThermoFinnigan Surveyor Plus photodiode array detector (PDA), a YMC-Pack ODS-AQ analytical column (length = 250 mm, inner diameter = 4.6 mm, particle size = 5µm) and Finnigan LCQ Deca mass spectrometer (HPLC-MS). Mass spectra were obtained using electro-spray ionization (± ESI) with 5kV spray voltage, 275 °C capillary temperature, and a 5.5 mm inner diameter capillary. Sheath and sweep gas flow rates were 40 and 20 (arbitrary units as used by the control software Finnigan Xcaliber V 1.3), respectively. Eluant composition was 0.1% formic acid in ACN (solvent a), 10 mM ammonium formate (solvent b) and 10 mM ammonium formate in 90% ACN (solvent c). The mobile phase elution (1 ml min^{-1}) was isocratic (with a solvent ratio a:b:c of 4:72:24 for 13.5 min, ramped to 4:0:96 over 4.5 min, and isocratic (4:0:96) for 17 min. Aliquots (200 µl) from the fMLP matrix were removed temporally, spiked with 2 µg of *boc*-lysine (2-(*tert*-butoxycarbonylamino)-6-aminohexanoic acid) internal standard, and 20 µl full-loop injections were made. fMLP relative retention was 1.17 ± 0.2 min and the method limit of detection 1.7 ± 2 ng was achieved in negative mode using select ion monitoring of the mass-to-charge ratio (*m/z*) 436 and 499 (**Supplementary Fig. 9**).

The UV light fluorescence spectroscopy detection of fMLP was done with a spectrofluorimeter (FluoroMax-3, HORIBA Jobin Yvon). The excitation wavelength was 240 nm and the fluorescence emission spectrum was recorded in the range from 260 nm to 350 nm (**Supplementary Fig. 10**). The peak region of this spectrum around 284 nm was used for the quantification of the concentration of fMLP.

Gradient chamber assay. Fibronectin (from bovine plasma; Sigma) was dissolved in sterile water at 1 mg/ml concentration for 1 h at room temperature and then diluted 1:5 in sterile filtered calcium and magnesium–free (Ca/Mg-free) PBS (DPBS; VWR). We plated 100 µl of the diluted fibronectin solution on a coverslip and incubated for 1 h at room temperature. Then the fibronectin was aspirated and the coverslips were washed twice with Ca/Mg-free PBS. Then 200 µl of modified HBSS (mHBSS: HBSS (Invitrogen) with 0.2% (wt/vol) BSA (low endotoxin) (Sigma-Aldrich)) were plated on the coverslip for 5 min. Differentiated HL-60 cells were washed once (400*g* for 1 min) in mHBSS and plated on the coverslip and incubated for 20 min at 37 °C in a humid chamber. Unbound cells were washed three times with mHBSS[31].

doi:10.1038/nmeth.1400

The coverslip was mounted in a Zigmond gradient chamber. One reservoir of the chamber was filled with mHBSS buffer containing chemoattractant and the other reservoir with plain mHBSS buffer. As chemoattractant we either used fMLP directly (as purchased from Sigma-Aldrich) or we used fMLP loaded into and subsequently released from PLGA beads. For collecting the released fMLP, PLGA beads loaded with fMLP were dispersed in mHBSS buffer. After a certain amount of time (30 min or 60 min), the beads were centrifuged (at 2,300*g* for 5 min) and the supernatant containing the released fMPL was collected. This supernatant was diluted in buffer (mHBSS) and filled into one reservoir of a Zigmond gradient chamber[22] and pure control buffer (mHBSS) was filled into the other reservoir. The cellular response was recorded with time-lapse microscopy on a Nikon TE-2000 microscope with a ×10 phase contrast lens at a frame rate of six frames per minute.

Single-cell stimulation experiments. Fibronectin (from bovine plasma, Sigma-Aldrich) was dissolved in sterile water at 1 mg ml^{-1} concentration for 1 h at room temperature and then diluted 1:5 in sterile filtered Ca/Mg-free PBS (DPBS; VWR). We plated 125 µl of the diluted fibronectin solution on a coverslip and incubated for 1 h at room temperature. Afterwards the fibronectin was aspirated and the coverslips were washed twice with RPMI 1640 medium (RPMI; Cellgro) containing 1% FBS and 25 mM Hepes. 100 µl of differentiated HL-60 cells at a concentration of about 1.2×10^6 cells ml^{-1} were plated on the coverslip and incubated for 20 min at 37 °C in a humid chamber. Unbound cells were washed three times with RPMI. PLGA particles loaded with fMLP were dispersed in RPMI. The size distribution of the beads was narrowed by the following washing procedure: 1 ml of the RPMI medium containing 1 mg of beads was centrifuged in 1.5 ml tubes at 1,000*g* for 3 min. The supernatant was discarded and the pellet was redispersed in 1 ml RPMI. This solution was then diluted 1:500 in RPMI and plated on the coverslip with the cells. The coverslips were mounted into the Nikon TE-2000 microscope equipped with holographic optical tweezers. Individual PLGA particles were trapped and manipulated at laser powers of around 5 mW in the focal plane.

We imaged our samples using differential interference contrast (DIC) microscopy using an inverted microscope (TE2000, Nikon) with an oil immersion objective lens (Apochromat TIRF ×100, NA 1.49; Nikon). The images were recorded with a charge-coupled device (CCD) camera (ORCA ER; Hamamatsu) at a frame rate of 1 Hz. To manipulate the microparticles, we used holographic optical tweezers. A liquid crystal spatial light modulator (HEO 1080P, Holoeye) was used as a diffractive optical element for a laser beam with a wavelength of 1,064 nm (Compass 4W CW laser; Coherent). The spatial light modulator was placed in a conjugate focal plane of the microscope objective. The computer-controlled holographic patterns on the spatial light modulator dephased the laser beam spatially to allow the creation of multiple laser spots in the focal plane of the microscope. The real-time manipulation of the microparticles and the image acquisition was controlled by software implemented in Matlab (Mathworks).

Microthermometry and spinning disk confocal microscopy. PLGA particles were suspended in a solution of Rhodamine B (0.05 mM). Rhodamine B is a temperature-sensitive fluorescent dye that shows a decrease in fluorescence by 2.3% per 1 °C temperature increase. The sample was excited with a 561 nm laser and the emitted fluorescence was imaged with a spinning disk confocal microscope (Nikon Eclipse Ti microscope equipped with a spinning disk confocal head and an Andor iXon EM-CCD camera). Ratiometric imaging was done by dividing an image of a particle in an optical trap at high laser power (230 mW in focal plane) by a reference image at 0 mW laser power. The resulting ratio image was subtracted from 1 and then multiplied by a factor of −44 to derive the temperature distribution around the bead. An offset was added to normalize the background temperature to the room temperature of 24 °C.

YFP actin transfection. YFP-actin was amplified by PCR (polymerase chain reaction) using the following sets of primers: 5′-AACGAATTCATGGTGAGCAAGGGCGAGGA-3′ and 5′-GCGGAATTCCTAGAAGCATTTGCGGTGGACG-3′ before it was inserted into pCMV vector to generate pCMV-YFP-actin plasmid. For transient transfection of HL-60 cells, 2 million DMSO-differentiated HL-60 cells were electroporated with 1.5 µg endotoxin-free plasmids (pCMV-YFP-actin) using the Nucleofector Kit V with the Amaxa Nucleofector system (Lonza) according to the manufacturer's instructions. The cells were then cultured for 24 h in Iscove's Modified DMEM containing 20% FBS before imaging.

31. Servant, G., Weiner, O.D., Neptune, E.R., Sedat, J.W. & Bourne, H.R. Dynamics of a chemoattractant receptor in living neutrophils during chemotaxis. *Mol. Biol. Cell* **10**, 1163–1178 (1999).